


Impact of silica environment on hyperfine interactions in ϵ -Fe₂O₃ nanoparticles

Lenka Kubíčková¹  · Jaroslav Kohout¹ · Petr Brázda² · Miroslav Veverka² · Tomáš Kmječ¹ · Denisa Kubániová¹ · Petr Bezdička³ · Mariana Klementová² · Eva Šantavá² · Karel Závěta¹

Published online: 15 November 2016
© Springer International Publishing Switzerland 2016

Abstract Magnetic nanoparticles have found broad applications in medicine, especially for cell targeting and transport, and as contrast agents in MRI. Our samples of ϵ -Fe₂O₃ nanoparticles were prepared by annealing in silica matrix, which was leached off and the bare particles were then coated with amorphous silica layers of various thicknesses. The distribution of particle sizes was determined from the TEM pictures giving the average size ~ 20 nm and the thickness of silica coating ~ 5 ; 8; 12; 19 nm. The particles were further characterized by the XRPD and DC magnetic measurements. The nanoparticles consisted mainly of ϵ -Fe₂O₃ with admixtures of ~ 1 % of the α phase and less than 1 % of the γ phase. The hysteresis loops displayed coercivities of ~ 2 T at room temperature. The parameters of hyperfine interactions were derived from transmission Mössbauer spectra. Observed differences of hyperfine fields for nanoparticles in the matrix and the bare ones are ascribed to strains produced during cooling of the composite. This interpretation is supported by slight changes of their lattice parameters and increase of the elementary cell volume deduced from XRD. The temperature dependence of the magnetization indicated a two-step magnetic transition of the ϵ -Fe₂O₃ nanoparticles spread between ~ 85 K and ~ 150 K, which is slightly modified by remanent tensile stresses in the case of nanoparticles in the matrix. The subsequent coating of the bare particles by silica produced no further change in hyperfine parameters, which indicates that this procedure does not modify magnetic properties of nanoparticles.

This article is part of the Topical Collection on *Proceedings of the International Conference on Hyperfine Interactions and their Applications (HYPERFINE 2016), Leuven, Belgium, 3-8 July 2016* Edited by Kristiaan Temst, Stefaan Cottenier, Lino M. C. Pereira and André Vantomme

✉ Lenka Kubíčková
sagittaria.64@gmail.com

¹ Faculty of Mathematics and Physics, Charles University in Prague, V Holešovičkách 2, 180 00 Prague, Czech Republic

² Institute of Physics of the AS CR, v.v.i., Na Slovance 2, 182 21 Prague, Czech Republic

³ Institute of Inorganic Chemistry of the AS CR, v.v.i., Husinec-Řež 1001, 250 68 Řež, Czech Republic

Keywords Iron oxide · Polymorph of ferric oxide · ^{57}Fe Mössbauer spectrometry · Ferrimagnetic nanoparticles · Giant coercive field · Spin-reorientation transition

1 Introduction

Magnetic nanoparticles (MNs) have attracted due attention for their extraordinary properties so different from the bulk material, which enable their plentiful technological applications. Over last decades, MNs have come into broad use in biomedicine, for both *in vivo* (contrast agents in magnetic resonance imaging – MRI, hyperthermia, targeted drug delivery and tissue repair etc.) and *in vitro* (cell separation) applications [1]. Crucial qualities of MNs for medical utilization are a well-controlled size of MNs along with a narrow size distribution, high effectivity and most importantly, low toxicity. To avoid agglomeration and prevent the release of toxic ions, improving thus the MNs tolerance in the living organism, the MNs are often coated with inert materials, e.g. amorphous silica (SiO_2), gold layer or organic polymers (polyethylene glycol, PEG) [2, 3]. Among MNs, the superparamagnetic iron oxide nanoparticles have aroused considerable interest due to their good chemical stability and high biocompatibility [4].

Nanosized $\epsilon\text{-Fe}_2\text{O}_3$ represents a remarkable phase of ferric oxide, differing from commonly known $\alpha\text{-Fe}_2\text{O}_3$ and $\gamma\text{-Fe}_2\text{O}_3$ by e.g. high magnetocrystalline anisotropy resulting in giant coercive field of 2 T [5] at room temperature and high blocking temperature of ferrimagnetic nanoparticles. It is considered to be a metastable phase of ferric oxide with scarce natural abundance and may be prepared only in nanosized form or as a thin film [6]. The crystal structure of $\epsilon\text{-Fe}_2\text{O}_3$ is orthorhombic with space group $\text{Pna}2_1$ [7], lattice parameters $a = 5.1019(3)$ Å, $b = 8.7807(6)$ Å, $c = 9.4661(5)$ Å [8] and eight formula units per unit cell. Four non-equivalent cation positions are octahedrally (Fe_{DO1} , Fe_{DO2} , Fe_{RO}) and tetrahedrally (Fe_{T}) coordinated, four sublattice magnetizations are (anti)parallel to a -axis [9]. $\epsilon\text{-Fe}_2\text{O}_3$ exhibits a magnetic transition from the paramagnetic to the ferrimagnetic state at the Curie temperature of ~ 490 K [7] and another two-step spin reorientation transition in the temperature range 100–153 K [10]. For a comprehensive review on this material see Tuček et al. [11].

In this work, X-Ray Powder Diffraction (XRPD), Transmission Electron Microscopy (TEM), DC magnetic measurements and ^{57}Fe Transmission Mössbauer Spectroscopy (MS) were employed in a study of $\epsilon\text{-Fe}_2\text{O}_3$ nanoparticles coated with amorphous silica layer with respect to the potential use of this promising material in MRI. We focused on the influence of the thickness of silica coating on hyperfine parameters of ^{57}Fe nuclei in $\epsilon\text{-Fe}_2\text{O}_3$ nanoparticles.

2 Sample preparation

Due to its metastability, the synthesis of pure $\epsilon\text{-Fe}_2\text{O}_3$ without admixtures of other phases of ferric oxide is difficult. Lately, the strategy of preparation of nanocrystalline $\epsilon\text{-Fe}_2\text{O}_3$ employing a supporting silica matrix with well-defined pores has been widely accepted as the most convenient method, improving the phase composition of the nanoparticles [10]. The preparation of $\epsilon\text{-Fe}_2\text{O}_3$ individual silica coated nanoparticles consisted of the following steps [12]:

1. preparation of mesoporous amorphous SiO_2 template with pores ~ 5 nm

2. impregnation of this template by aqueous solution of iron(III) nitrate nonahydrate $\text{Fe}(\text{NO}_3)_3 \cdot 9 \text{H}_2\text{O}$
3. annealing at temperatures of about 1320 K
4. leaching off the silica matrix by NaOH after the crystallization of nanoparticles
5. coating the particles by amorphous silica in TEOS (tetraethyl-orthosilicate) solution (adjusted from [13]).

The last step of the preparation is introduced in order to reduce their toxicity and degradability in living organisms.

Six types of $\epsilon\text{-Fe}_2\text{O}_3$ samples were used for further study: nanoparticles in the silica matrix (labelled $\epsilon\text{-Fe}_2\text{O}_3\text{-m}$), bare ($\epsilon\text{-Fe}_2\text{O}_3\text{-0}$) and covered with silica coating of various thicknesses (four samples $\epsilon\text{-Fe}_2\text{O}_3\text{-5nm}$, $\epsilon\text{-Fe}_2\text{O}_3\text{-8nm}$, $\epsilon\text{-Fe}_2\text{O}_3\text{-12nm}$ and $\epsilon\text{-Fe}_2\text{O}_3\text{-19nm}$ numbered according to the thickness of the silica coating obtained from TEM images as indicated below).

3 Experimental

XRPD of the samples was accomplished with PANalytical XPertPRO MPD diffractometer with the $\text{Cu K}\alpha$ radiation in the 2θ range $10^\circ\text{-}95^\circ$ in Bragg-Brentano reflex geometry. The data analysis was carried out using the WinPLOTR software [14]. The evaluation of phase composition was based on structural models of $\epsilon\text{-Fe}_2\text{O}_3$ [15], $\alpha\text{-Fe}_2\text{O}_3$ [16] and $\gamma\text{-Fe}_2\text{O}_3$ [12]. The apparent crystallite size was obtained from the analysis of diffraction profiles using the pseudo-Voigt profile shapes.

TEM was carried out with Phillips CM120 microscope using the acceleration voltage 120 kV. Bright field images of nanoparticles deposited on a carbon film were analysed to acquire the distribution of particle sizes and the thickness of silica coating (if present).

Hysteresis loops up to 5 T were obtained at 300 K using the SQUID magnetometer MPMS XL-7 by Quantum Design (QD). The temperature dependence of magnetization after cooling in zero (ZFC) and non-zero (FC) external magnetic field was measured in the SQUID magnetometer by QD.

Transmission Mössbauer spectra were acquired with a $^{57}\text{Co/Rh}$ source with constant acceleration in zero external magnetic field, calibration of velocities and isomer shifts was related to $\alpha\text{-Fe}$ at room temperature of 296 K. Spectra were analysed using CONFIT software [17].

4 Results and discussion

Figure 1 shows XRPD patterns of bare and coated nanoparticles. XRPD proved $\epsilon\text{-Fe}_2\text{O}_3$ to be the major phase in the samples with 98(1) % occurrence, followed by 1.5(5) % of $\alpha\text{-Fe}_2\text{O}_3$ and less than 1 % of $\gamma\text{-Fe}_2\text{O}_3$. The lattice parameters of $\epsilon\text{-Fe}_2\text{O}_3$ of all samples are shown in Table 1, along with the mean coherent diffraction domain size. In samples with silica coating, there is a noticeable broad peak of SiO_2 in the range of 2θ approximately $20^\circ\text{-}36^\circ$, which was included in the background. Presently the signal of $\epsilon\text{-Fe}_2\text{O}_3$ decreased with the rising content of silica, resulting in higher inaccuracy in determination of lattice parameters of the particles. In comparison to the bare nanoparticles, nanoparticles in silica matrix evinced slight changes of the lattice parameters and an increase of the elementary cell volume (see Table 1).

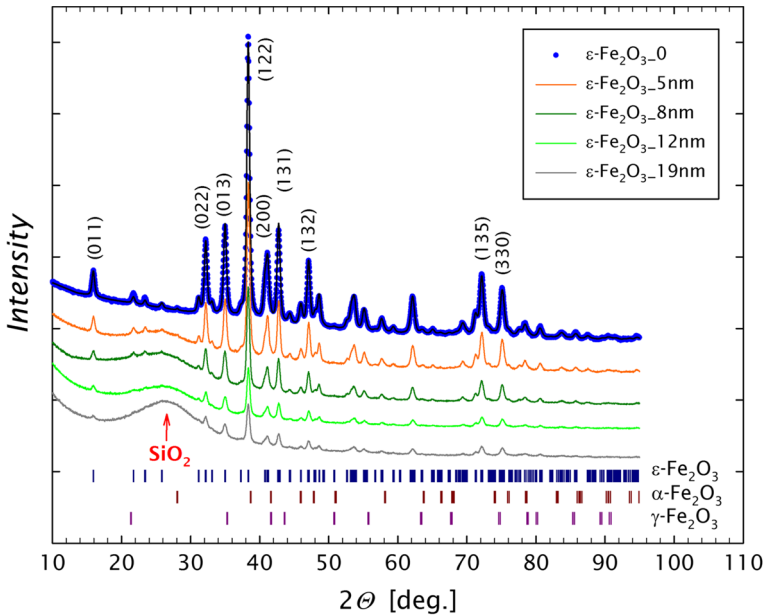


Fig. 1 X-ray powder diffraction pattern of the bare and coated nanoparticles. Positions of diffraction maxima of considered polymorphs are marked by vertical bars under the diffractograms. The amorphous peak of silica present in the coating is indicated by an arrow

Table 1 An overview of examined samples with results obtained from XRPD and TEM analysis: t – indicated types of samples are m - in matrix, b - bare, c - coated with silica; a, b, c - lattice parameters of ϵ -Fe₂O₃, V - volume of elementary cell as calculated from lattice parameters, CDDS - mean coherent diffraction domain size, d₀ - median of a characteristic particle diameter, PDI - polydispersity index, l₀ - thickness of silica coating (if present), σ_l – specific magnetization in 5 T

sample	t	a [Å]	b [Å]	c [Å]	V [Å ³]	CDDS [nm]	d ₀ [nm]	PDI	l ₀ [nm]	σ_l [emu/g]
ϵ -Fe ₂ O ₃ -m	m	5.096(3)	8.810(9)	9.469(8)	425.1(6)	18(1)	22	0.7	-	-
ϵ -Fe ₂ O ₃ -0	b	5.0906(3)	8.7871(8)	9.4765(6)	423.90(5)	18(1)	18	0.8	0	16.37
ϵ -Fe ₂ O ₃ -5nm	c	5.0900(3)	8.7853(7)	9.4767(6)	423.77(5)	20(1)	23	0.7	4.6(9)	10.76
ϵ -Fe ₂ O ₃ -8nm	c	5.0894(4)	8.7852(9)	9.4761(7)	423.69(6)	19(1)	21	0.9	8(1)	6.38
ϵ -Fe ₂ O ₃ -12nm	c	5.0882(6)	8.783(1)	9.473(1)	423.35(8)	19(1)	18	0.8	12(1)	4.15
ϵ -Fe ₂ O ₃ -19nm	c	5.0895(7)	8.784(2)	9.476(1)	423.6(1)	20(1)	20	0.8	19(1)	2.17

An overview of TEM bright field images of the samples is given in Fig. 2. The distribution of particle sizes acquired by analysis of TEM images was fitted by the lognormal distribution, which is well justified for particles growing in the presence of significant drift and/or diffusion [18]:

$$P(d) = \frac{1}{\sqrt{2\pi}\sigma d} e^{-\frac{\ln^2\left(\frac{d}{d_0}\right)}{2\sigma^2}}, \tag{1}$$

the dispersion of the particles is characterised by the polydispersity index:

$$PDI = \frac{\sqrt{\langle d^2 \rangle - \langle d \rangle^2}}{\langle d \rangle} = \sqrt{e^{\sigma^2} - 1}, \tag{2}$$

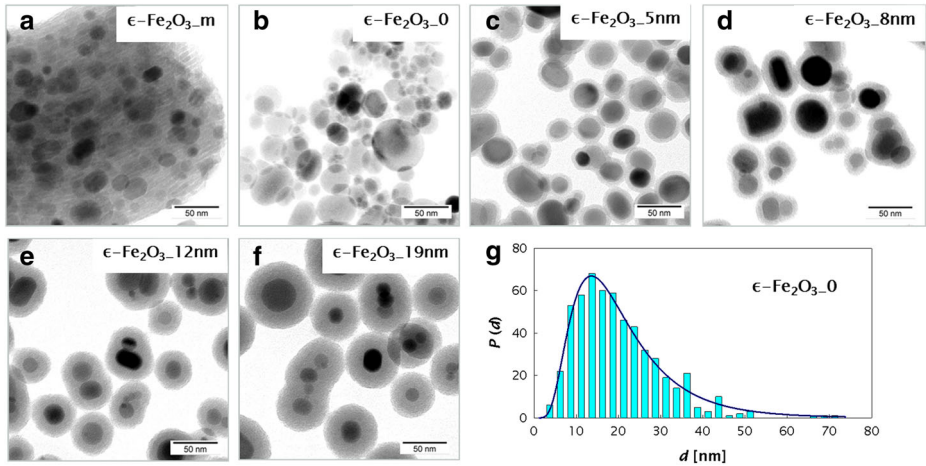


Fig. 2 Representative TEM bright field images of the $\epsilon\text{-Fe}_2\text{O}_3$ nanoparticles (a) in silica matrix, (b) bare and (c)–(f) coated with silica layer of various thicknesses. A typical particle histogram (here for the sample of bare nanoparticles $\epsilon\text{-Fe}_2\text{O}_3_0$) fitted by log-normal distribution (1) is shown in (g)

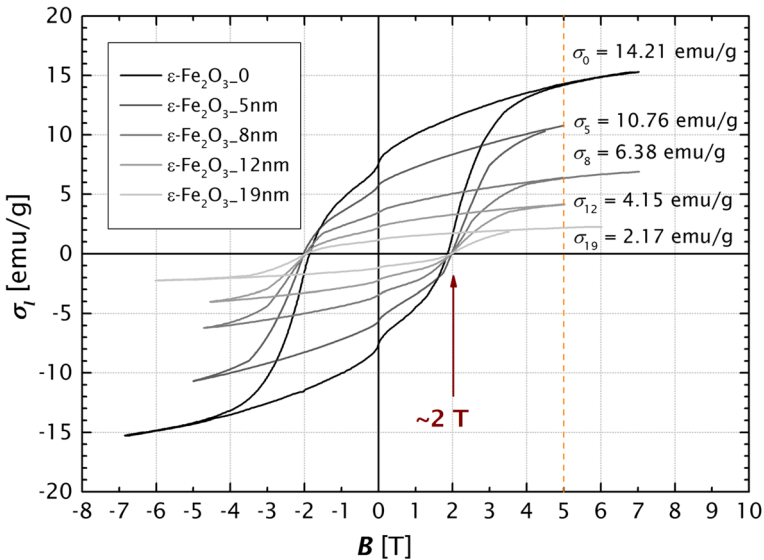


Fig. 3 Hysteresis loops of bare and coated nanoparticles measured at 300 K. The coercive field of 2 T is highlighted; the differences in specific magnetization of the samples reflect the various content of silica

while normal distribution was used to fit the thickness of the silica coating:

$$P(l) = \frac{1}{\sqrt{2\pi}\sigma} e^{-\frac{(l-l_0)^2}{2\sigma^2}} \tag{3}$$

The histogram of the distribution of particles in the sample $\epsilon\text{-Fe}_2\text{O}_3_0$ was chosen as a representative of all samples and is given in Fig. 2.

Table 2 Hyperfine parameters of ϵ -Fe₂O₃ for non-equivalent cation positions of ⁵⁷Fe in the core and in the shell determined for all samples from the Transmission Mössbauer Spectroscopy

	sample	Cation positions in the core				Cation positions in the shell			
		Fe _{DO1}	Fe _{DO2}	Fe _{RO}	Fe _T	Fe _{DO1}	Fe _{DO2}	Fe _{RO}	Fe _T
<i>IS</i> [mm.s ⁻¹]	ϵ -Fe ₂ O ₃ _m	0.41(4)	0.38(3)	0.40(2)	0.23(3)	0.41(4)	0.38(3)	0.40(2)	0.23(3)
	ϵ -Fe ₂ O ₃ _0	0.41(3)	0.36(3)	0.39(2)	0.23(2)	0.41(3)	0.36(3)	0.39(2)	0.23(2)
	ϵ -Fe ₂ O ₃ _5nm	0.41(3)	0.36(3)	0.39(2)	0.22(2)	0.41(3)	0.36(3)	0.39(2)	0.22(2)
	ϵ -Fe ₂ O ₃ _8nm	0.39(3)	0.37(3)	0.39(2)	0.23(2)	0.37(3)	0.39(3)	0.39(2)	0.23(2)
	ϵ -Fe ₂ O ₃ _12nm	0.41(3)	0.36(3)	0.39(2)	0.23(2)	0.41(3)	0.36(3)	0.39(2)	0.23(2)
	ϵ -Fe ₂ O ₃ _19	0.41(3)	0.37(3)	0.40(2)	0.24(2)	0.41(3)	0.37(3)	0.40(2)	0.24(2)
<i>QS</i> [mm.s ⁻¹]	ϵ -Fe ₂ O ₃ _m	-0.19(7)	-0.30(7)	-0.01(3)	-0.16(3)	0	0	0	0
	ϵ -Fe ₂ O ₃ _0	-0.17(4)	-0.31(4)	0.01(3)	-0.14(3)	0	0	0	0
	ϵ -Fe ₂ O ₃ _5nm	-0.16(4)	-0.31(4)	0.01(3)	-0.15(3)	0	0	0	0
	ϵ -Fe ₂ O ₃ _8nm	-0.15(3)	-0.33(4)	0.02(3)	-0.14(3)	0	0	0	0
	ϵ -Fe ₂ O ₃ _12nm	-0.17(4)	-0.30(4)	0.01(3)	-0.16(3)	0	0	0	0
	ϵ -Fe ₂ O ₃ _19nm	-0.16(3)	-0.31(3)	0.02(3)	-0.15(3)	0	0	0	0
<i>B_{hf}</i> [T]	ϵ -Fe ₂ O ₃ _m	45.1(4)	44.6(4)	39.4(2)	26.0(2)	42.4(6)	33.8(4)	37.1(5)	20.6(5)
	ϵ -Fe ₂ O ₃ _0	45.2(2)	44.8(2)	39.7(2)	26.6(2)	42.6(4)	35.9(4)	38.7(4)	23.1(4)
	ϵ -Fe ₂ O ₃ _5nm	45.2(2)	44.9(2)	39.8(2)	26.6(2)	42.0(4)	35.4(4)	38.1(4)	23.0(4)
	ϵ -Fe ₂ O ₃ _8nm	45.3(3)	44.9(3)	39.8(2)	26.6(2)	41.6(4)	34.8(5)	37.8(4)	22.9(4)
	ϵ -Fe ₂ O ₃ _12nm	45.3(2)	45.0(2)	39.7(2)	26.6(2)	41.4(4)	34.4(4)	37.5(4)	23.1(4)
	ϵ -Fe ₂ O ₃ _19nm	45.2(2)	45.0(2)	39.7(2)	26.6(2)	42.0(4)	35.2(4)	37.8(4)	22.8(4)

The same isomer shifts for the corresponding components in the shell and in the core were supposed, and a random canting of the shell spins, which averages to zero quadrupolar shifts in the shell. *IS* – isomer shift, *QS* – quadrupole splitting, *B_{hf}* – hyperfine magnetic field

Median of the equivalent diameter of particles and the thickness of silica coating (if present) are summarised together with XRPD results in Table 1. The median of the equivalent diameter and the mean coherent diffraction domain size of the samples are in a quantitative agreement.

The hysteresis loops of the samples are depicted in Fig. 3. The coercive field of 2 T was confirmed for all samples, and the presence of less than 1 % of ferrimagnetic γ -Fe₂O₃ impurities was estimated from the kink of magnetization at zero magnetic field. As apparent from the Fig. 3, specific magnetization decreases with increasing thickness of silica coating.

The information on the hyperfine fields and orientations of the local magnetic moments were derived from the Mössbauer spectra considering the core-shell model [19, 20] for the ϵ -Fe₂O₃ nanoparticles, assuming an essentially collinear ordering of the moments in the core and a random one in the shell. We supposed the same isomer shifts for the corresponding components in the shell and in the core of ϵ -Fe₂O₃ and a random canting of the spins in the shell, which averages to zero quadrupolar shifts in the shell. The results of isomer shift, quadrupole splitting and hyperfine magnetic field on ⁵⁷Fe nuclei are given in Table 2, a typical MS spectrum of ϵ -Fe₂O₃ with the decomposition to the contributions of both core and shell for all non-equivalent cation sites is depicted in Fig. 4. The thickness of the shell layer

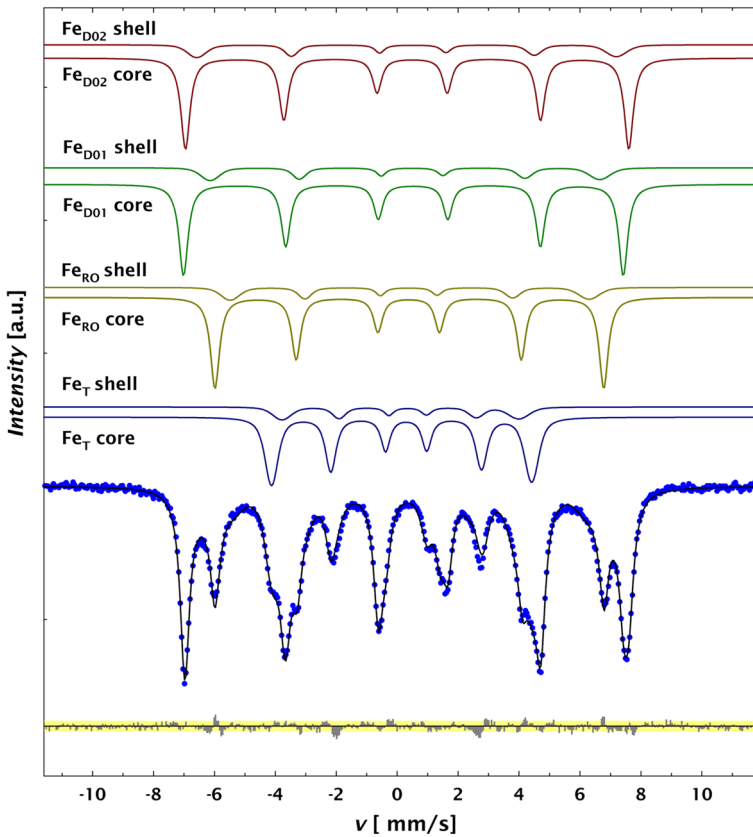


Fig. 4 A representative Mössbauer spectrum of $\epsilon\text{-Fe}_2\text{O}_3$ ($\epsilon\text{-Fe}_2\text{O}_3\cdot 0$) acquired at room temperature (296 K) in zero external magnetic field. The decomposition into fitted contributions of all non-equivalent cation positions in both core and shell is given above the experimental spectrum. The difference spectrum (fit subtracted from experimental values) is indicated below, the *yellow area* denotes the statistical limit for deviations when the Poisson distribution is supposed

1.0(3) nm was estimated from the relative intensities of the shell components in Mössbauer spectra considering the simplifying assumptions of the same Lamb-Mössbauer factors of iron atoms in the core and the shell and constant thickness of the shell for all nanoparticles in the sample. It was obtained by solving the following equation:

$$\frac{I_{shell}}{I_{shell} + I_{core}} = \frac{V - V_{core}(t)}{V}, \tag{4}$$

where I_{shell} and I_{core} are the relative intensities of the shell and core components, respectively, t is the thickness of the shell,

$$V = \int_0^\infty P(d) \frac{\pi}{6} d^3 dd \quad \text{and} \quad V_{core}(t) = \int_0^\infty P(d) \frac{\pi}{6} (d - 2t)^3 dd \tag{5}$$

are the overall volume of the nanoparticles and the volume of only the core component, respectively.

In comparison to the bare nanoparticles, nanoparticles in silica matrix displayed convincingly lower hyperfine magnetic field in all Fe cation positions. Considering the fact that

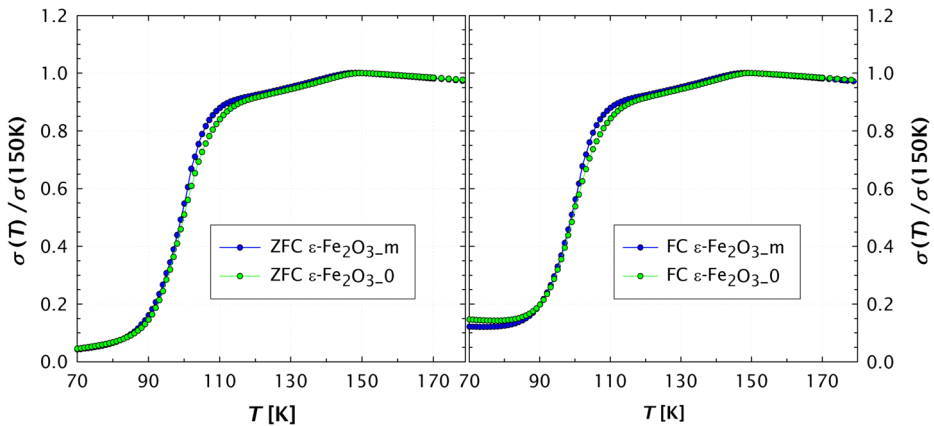


Fig. 5 Temperature dependence of magnetization of nanoparticles in the silica matrix and the bare ones - ZFC and FC curves, normalized in relation to the magnetization at 150 K. A slightly steeper increase in magnetization of particles in the matrix indicates influence of tensile stresses in the composite on the magnetic transition

the hyperfine magnetic field on ^{57}Fe nuclei in $\epsilon\text{-Fe}_2\text{O}_3$ increases with increasing pressure (J. Kohout et al., In-situ high pressure studies of $\epsilon\text{-Fe}_2\text{O}_3$ nanopowder, to be published), we presume that there are tensile stresses present in the composite. The stresses probably stem from the tension produced during cooling of the composite as a result of different volumetric thermal expansion coefficient of the particles and silica. This interpretation is in agreement with slight changes of the lattice parameters and an increase of the elementary cell volume deduced from XRPD.

The ZFC and FC curves of relative magnetization related to magnetization at 150 K for nanoparticles in silica matrix and the bare ones are gathered in Fig. 5. A two-step magnetic transition in the temperature range 100–153 K described in Kohout et al. [10] was confirmed also for our samples, albeit with the first step in the range $\sim 85\text{--}110$ K and the second at $\sim 110\text{--}150$ K. The increase in magnetization of the nanoparticles in the silica matrix is slightly steeper, indicating influence of tensile stresses in the composite on the magnetic transition.

According to our data, there is no influence of subsequent silica coating on the hyperfine interactions in $\epsilon\text{-Fe}_2\text{O}_3$ nanoparticles. This is probably not the case in Taboada et al. [9], where the nanoparticles of $\epsilon\text{-Fe}_2\text{O}_3$ with silica coating were prepared by annealing of $\gamma\text{-Fe}_2\text{O}_3$ nanoparticles embedded in silica. We presume that tensile stresses must be present in the composite synthesised this way. Our results also indicate that magnetic properties of the nanoparticles remain unchanged when processed by subsequent coating with the prospect of their biomedical application, e.g. as contrast agents in MRI or as mediators of targeted cell and drug transport.

5 Summary

Systems of $\epsilon\text{-Fe}_2\text{O}_3$ nanoparticles in silica matrix, bare and coated with amorphous silica layer with various thicknesses were studied using XRPD, TEM, DC magnetic measurements and MS. The samples of nanoparticles prepared by the described procedure consisted

mainly of the ϵ -Fe₂O₃ with admixtures of about 1 % of α phase and less than 1 % of the γ phase. The size of nanoparticles was \sim 20 nm and the thickness of silica coating \sim 5; 8; 12; 19 nm. The hysteresis loops at room temperature displayed coercivities of \sim 2 T typical for the magnetic order of ϵ -Fe₂O₃ above the spin reorientation transition at \sim 150 K. The differences in lattice parameters and in hyperfine parameters of the Mössbauer spectra between particles in the matrix and the bare ones are ascribed to the tensile stress produced during cooling of the composite. The temperature dependence of the magnetization manifested a two-step magnetic transition spread between \sim 85 K and \sim 150 K, which is modified by the stress in the composite of nanoparticles in the silica matrix. The coating of the bare particles by silica produced no further change in hyperfine parameters, which suggests that subsequent coating by silica does not influence magnetic properties of MNs intended for further use in biomedicine.

Acknowledgments This work was supported by the Czech Science Foundation under the grant 16-04340S.

References

1. Laurent, S., Forge, D., Port, M., Roch, A., Robic, C., Elst, L.V., Muller, R.N.: Magnetic iron oxide nanoparticles: synthesis, stabilization, vectorization, physicochemical characterizations, and biological applications (vol 108, pg 2064, 2008). *Chem. Rev.* **110**(4), 2574 (2010). doi:[10.1021/Cr900197g](https://doi.org/10.1021/Cr900197g)
2. Liu, G., Gao, J., Ai, H., Chen, X.: Applications and potential toxicity of magnetic iron oxide nanoparticles. *Small* **9**(9–10), 1533–1545 (2013). doi:[10.1002/smll.201201531](https://doi.org/10.1002/smll.201201531)
3. Sun, C., Lee, J.S.H., Zhang, M.: Magnetic nanoparticles in MR imaging and drug delivery. *Adv. Drug Deliv. Rev.* **60**(11), 1252–1265 (2008). doi:[10.1016/j.addr.2008.03.018](https://doi.org/10.1016/j.addr.2008.03.018)
4. Tartaj, P., Morales, M.a.d.P., Veintemillas-Verdaguer, S., González Carretero, T., Serna, C.J.: The preparation of magnetic nanoparticles for applications in biomedicine. *J. Phys. D: Appl. Phys.* **36**(13), R182–R197 (2003). doi:[10.1088/0022-3727/36/13/202](https://doi.org/10.1088/0022-3727/36/13/202)
5. Tseng, Y.C., Souza-Neto, N.M., Haskell, D., Gich, M., Frontera, C., Roig, A., Van Veenendaal, M., Nogués, J.: Nonzero orbital moment in high coercivity ϵ -Fe₂O₃ and low-temperature collapse of the magnetocrystalline anisotropy. *Phys. Rev. B - Condens. Matter Mater. Phys.* **79**(9), 1–6 (2009). doi:[10.1103/PhysRevB.79.094404](https://doi.org/10.1103/PhysRevB.79.094404)
6. Gich, M., Fina, I., Morelli, A., Sánchez, F., Alexe, M., Gázquez, J., Fontcuberta, J., Roig, A.: Multiferroic Iron oxide thin films at room temperature. *Adv. Mater. (Deerfield Beach Fla.)* **3**(111), 4645–4652 (2014). doi:[10.1002/adma.201400990](https://doi.org/10.1002/adma.201400990). <http://www.ncbi.nlm.nih.gov/pubmed/24831036>
7. Tronc, E., Chanéac, C., Jolivet, J.: Structural and magnetic characterization of ϵ -Fe₂O₃. *J. Solid State Chem.* **139**(1), 93–104 (1998). doi:[10.1088/0953-8984/23/12/126003](https://doi.org/10.1088/0953-8984/23/12/126003). <http://www.sciencedirect.com/science/article/pii/S0022459698978173>
8. Sakurai, S., Jin, J., Hashimoto, K., Ohkoshi, S.I.: Reorientation phenomenon in a magnetic phase of ϵ -Fe₂O₃ Nanocrystal. *J. Phys. Soc. Japan* **74**(7), 1946–1949 (2005). doi:[10.1143/JPSJ.74.1946](https://doi.org/10.1143/JPSJ.74.1946)
9. Taboada, E., Gich, M., Roig, A.: Nanospheres of silica with an ϵ -Fe₂O₃ single crystal nucleus. *ACS Nano* **3**(11), 3377–3382 (2009). doi:[10.1021/nn901022s](https://doi.org/10.1021/nn901022s)
10. Kohout, J., Brázda, P., Závěta, K., Kubániová, D., Kmječ, T., Kubíčková, L., Klementová, M., Šantavá, E., Lančok, A.: The magnetic transition in ϵ -Fe₂O₃ nanoparticles: Magnetic properties and hyperfine interactions from Mössbauer spectroscopy. *J. Appl. Phys.* **117**(17), 17D505 (2015). doi:[10.1063/1.4907610](https://doi.org/10.1063/1.4907610). <http://scitation.aip.org/content/aip/journal/jap/117/17/10.1063/1.4907610>
11. Tuček, J., Zbořil, R., Namai, A., Ohkoshi, S.I.: ϵ -Fe₂O₃: An advanced nanomaterial exhibiting giant coercive field, millimeter-wave ferromagnetic resonance, and magnetoelectric coupling. *Chem. Mater.* **22**(24), 6483–6505 (2010). doi:[10.1021/cm101967h](https://doi.org/10.1021/cm101967h)
12. Brázda, P., Kohout, J., Bezdička, P., Kmječ, T.: α -Fe₂O₃ versus β -Fe₂O₃: Controlling the phase of the transformation product of ϵ -Fe₂O₃ in the Fe₂O₃/SiO₂ system. *Cryst. Growth Des.* **14**(3), 1039–1046 (2014). doi:[10.1021/cg4015114](https://doi.org/10.1021/cg4015114)
13. Stöber, W., Fink, A., Bohn, E.: Controlled growth of monodisperse silica spheres in the micron size range. *J. Colloid Interf. Sci.* **26**(1), 62–69 (1968). doi:[10.1016/0021-9797\(68\)90272-5](https://doi.org/10.1016/0021-9797(68)90272-5)
14. Roisnel, T., Rodriguez-Carvajal, J.: WinPLOTR: A windows tool for powder diffraction pattern analysis. *Mater. Sci. Forum* **378–381**, 118–123 (2001)

15. Gich, M., Frontera, C., Roig, A., Taboada, E., Molins, E., Rechenberg, H.R., Ardisson, J.D., Macedo, W.A.A., Ritter, C., Hardy, V., Sort, J., Skumryev, V., Nogues, J.: High and low-temperature crystal and magnetic structures of ϵ -Fe₂O₃ and their correlation to its magnetic properties. *Chem. Mater.* **18**, 3889–3897 (2006). doi:[10.1021/cm0609931](https://doi.org/10.1021/cm0609931). <http://arxiv.org/abs/cond-mat/0604677>
16. Machala, L., Tuček, J., Zbořil, R.: Polymorphous transformations of nanometric iron(III) oxide: A review. *Chem. Mater.* **23**(14), 3255–3272 (2011)
17. Žák, T., Jirásková, Y.: CONFIT: Mössbauer spectra fitting program. *Surf. Interf. Anal.* **38**, 710–714 (2006). doi:[10.1002/sia2285](https://doi.org/10.1002/sia2285)
18. Kiss, L.B., Söderlund, J., Niklasson, G.A., Granqvist, C.G.: New approach to the origin of lognormal size distributions of nanoparticles. *Nanotechnology* **1**, 25–28. doi:[10.1088/0957-4484/10/1/006](https://doi.org/10.1088/0957-4484/10/1/006). <http://stacks.iop.org/0957-4484/10/i=1/a=006?key=crossref.1abef74d8eebae4f850c722f3127f402> <http://iopscience.iop.org/0957-4484/10/1/006>
19. Bødker, F., Mørup, S., Linderoth, S.: Surface effects in metallic iron nanoparticles. *Phys. Rev. Lett.* **72**(2), 282–285 (1994). doi:[10.1103/PhysRevLett.72.282](https://doi.org/10.1103/PhysRevLett.72.282)
20. Coey, J.M.D.: Noncollinear spin arrangement in ultrafine ferrimagnetic crystallites. *Phys. Rev. Lett.* **27**(17), 1140–1142 (1971)